

Article

The Peptide TAT-I24 with Antiviral Activity against DNA Viruses Binds Double-Stranded DNA with High Affinity

Hanna Harant ^{1,*}, Siegfried Höfner ^{2,3}, Franz Kricek ⁴, Christine Ruf ⁴, Zsolt Ruzsics ^{5,6,7}, Hartmut Hengel ^{5,6,7} and Ivan J. D. Lindley ¹

¹ Pivaris BioScience GmbH, 1030 Vienna, Austria; ivanlindley@gmail.com

² VSC Research Center, TU Wien, 1040 Vienna, Austria; siegfried.hoefinger@tuwien.ac.at

³ Department of Physics, Michigan Technological University, Houghton, MI 49931, USA

⁴ NBS-C BioScience & Consulting GmbH, 1230 Vienna, Austria; franz.kricek@nbs-c.at (F.K.); christine.ruf@nbs-c.at (C.R.)

⁵ Institute of Virology, Medical Center—University of Freiburg, 79104 Freiburg, Germany; zsolt.ruzsics@uniklinik-freiburg.de (Z.R.); hartmut.hengel@uniklinik-freiburg.de (H.H.)

⁶ Faculty of Medicine, University of Freiburg, 79104 Freiburg, Germany

⁷ German Consulting Laboratory for HSV and VZV, Medical Center—University of Freiburg, 79104 Freiburg, Germany

* Correspondence: hanna.harant@pivaris-bioscience.at

Abstract: The peptide TAT-I24, composed of the 9-mer peptide I24 and the TAT (48-60) peptide, exerts broad-spectrum antiviral activity against several DNA viruses. The current model of the mode of action suggests a reduction of viral entry and also a possible interaction with the viral DNA upon virus entry. To further support this model, the present study investigates the DNA binding properties of TAT-I24. DNA binding was analysed by gel retardation of a peptide-complexed DNA, fluorescence reduction of DNA labelled with intercalating dyes and determination of binding kinetics by surface plasmon resonance. Molecular dynamics simulations of DNA-peptide complexes predict high-affinity binding and destabilization of the DNA by TAT-I24. The effect on viral DNA levels of infected cells were studied by real-time PCR and staining of viral DNA by bromodeoxyuridine. TAT-I24 binds double-stranded DNA with high affinity, leading to inhibition of polymerase binding and thereby blocking of *de novo* nucleic acid synthesis. Analysis of early steps of virus entry using a bromodeoxyuridine-labelled virus as well as quantification of viral genomes in the cells indicate direct binding of the peptide to the viral DNA. Saturation of the peptide with exogenous DNA can fully neutralize the inhibitory effect. The antiviral activity of TAT-I24 is linked to its ability to bind DNA with high affinity. This mechanism could be the basis for the development of novel antiviral agents.

Keywords: antiviral peptide; antimicrobial peptide (AMP); cell-penetrating peptide (CPP); peptide interaction; DNA viruses; DNA-binding peptide



Citation: Harant, H.; Höfner, S.; Kricek, F.; Ruf, C.; Ruzsics, Z.; Hengel, H.; Lindley, I.J.D. The Peptide TAT-I24 with Antiviral Activity against DNA Viruses Binds Double-Stranded DNA with High Affinity. *Biologics* **2021**, *1*, 41–60. <https://doi.org/10.3390/biologics1010003>

Academic Editor: Kai Hilpert

Received: 24 May 2021

Accepted: 7 June 2021

Published: 10 June 2021

Publisher's Note: MDPI stays neutral with regard to jurisdictional claims in published maps and institutional affiliations.



Copyright: © 2021 by the authors. Licensee MDPI, Basel, Switzerland. This article is an open access article distributed under the terms and conditions of the Creative Commons Attribution (CC BY) license (<https://creativecommons.org/licenses/by/4.0/>).

1. Introduction

Viral infections are a global threat and there is an unmet medical need for novel therapeutics acting against a wide range of viral targets. Strategies to identify such agents involve either modulation of the host cell response or identification of common viral molecules [1–3]. Intensive research has therefore been undertaken to identify novel modes of interference, which also includes the development of antiviral peptides. Several peptides with antiviral activity have been identified and a comprehensive overview of experimentally confirmed peptides is provided by the antiviral database AVPd [4]. Antiviral peptides are derived from natural sources, such as venom peptides or peptides from marine organisms, but can be also naturally occurring antimicrobial peptides (AMP), such as lactoferrin/lactoferricin, defensins or the cathelicidin LL-37 which are produced by higher

organisms as a response to infections [5–8]. For example, the defensin-derived peptide P9R exerts broad-spectrum antiviral activity against several viruses of the respiratory tract, including influenza virus, coronaviruses and rhinoviruses [9]. Other peptides with antiviral activity include synthetic polycationic peptides or peptide sequences identified in natural proteins. One example of an entry inhibitor is the peptide EB, derived from the signal sequence of fibroblast growth factor 4 and has been reported to inhibit infection by herpes simplex virus, vaccinia virus and influenza A virus [10,11]. Other antiviral peptides are the FluPep peptides, derived from Tkip, a mimetic for the suppressor of cytokine signalling (SOCS) protein, which targets influenza viruses and contains positively charged residues fused to a hydrophobic peptide [12].

Other approaches to identify antiviral peptides utilize rational design by in silico methods to find inhibitors of viral fusion proteins in enveloped viruses. A potent peptidic fusion inhibitor of the influenza virus has been designed based on complementarity determining region (CDR) loops of neutralizing antibodies against hemagglutinin [13]. Peptide fusion inhibitors of coronaviruses, such as SARS-CoV but also MERS-CoV, have been designed based on the heptad repeat region 2 of the coronavirus spike protein and can inhibit coronavirus infection [14,15]. Prediction models using the Wimley-White interfacial hydrophobicity scale (WWIHS) to search for membrane-interacting sequences [16] have led to the identification of potential entry inhibitors targeting viruses, such as dengue viruses, West Nile virus, coronavirus, cytomegalovirus, herpes simplex virus and Rift Valley fever virus [17]. Many peptides with antiviral activity share specific features such as high hydrophobicity and amphipathicity allowing them to partition into membranes. Such membrane-acting peptides can thus inhibit fusion and uptake of various viruses and could lead to the development of broad-spectrum inhibitors [18]. Several tools are available which can help to predict the antiviral potential of a peptide, such as AVPred [19] or Feature-Informed Reduced Machine Learning for Antiviral Peptide Prediction (FIRM-AVP) [20].

One example of a marketed drug is the viral fusion inhibitor enfuvirtide (Fuzeon[®]) approved for the treatment of HIV infections [21]. The second example is bulevirtide (Hepcludex[®]) which was recently approved for the treatment of chronic hepatitis D [22]. Both peptides target viral entry and are useful for the treatment of chronic viral infections.

We have recently reported the identification of the novel, broad-acting antiviral peptide TAT-I24. This peptide inhibits replication of multiple, taxonomically diverse double-stranded DNA viruses, including herpes simplex virus, cytomegalovirus, adenovirus type 5, SV40 polyomavirus and vaccinia virus. The proposed mode-of-action suggested that the peptide can affect early steps during or after viral entry but may also be internalised with the virus where it interacts with the viral genome to inhibit subsequent events such as viral gene expression [23]. The present study, therefore, aimed to pinpoint the hypothesised interaction of this peptide with double-stranded DNA and to elucidate its antiviral mechanism of action at the early stages of the viral life cycle.

2. Results

2.1. The 9-mer Peptide I24 Blocks RNA Synthesis and Initiation Complex Formation by T7 RNA Polymerase

The linear, 9-mer peptide I24 comprising the sequence CLAFYACFC (Figure 1) was identified as an inhibitor of "foreign" gene expression due to its ability to selectively block transcription from a transfected eukaryotic plasmid-DNA when added together with the DNA to the transfection reaction [23].

It was, therefore, speculated that the peptide directly binds DNA and prevents gene expression by blocking RNA polymerase binding and/or activity. To study RNA polymerase binding in vitro, the effect of I24 on RNA transcription by the T7 RNA polymerase was tested using a linearised plasmid-DNA containing the T7 promoter allowing the synthesis of an RNA with a size of 465 bases. At a concentration of 200 μ M, I24 fully inhibited RNA synthesis by the T7 RNA polymerase from the plasmid-DNA. As with the transfection system, where the peptide was only active when added directly to the transfection reagent, I24 only inhibited in vitro RNA synthesis when added simultaneously with the polymerase

while it was unable to inhibit RNA synthesis when added during ongoing transcription (Figure 2A). This indicates, that once the enzyme is actively transcribing, the peptide cannot inhibit RNA synthesis anymore. It was therefore examined whether binding of the T7 RNA polymerase to its promoter is inhibited by I24. In the presence of the initiator codon GTP, T7 RNA polymerase forms a complex with the T7 promoter which can be visualised by a DNase I footprint on the coding as well as non-coding strand [24,25]. A possible block of the T7 RNA polymerase transcription complex formation by I24 was therefore investigated using a PCR product end-labelled with 6-carboxyfluorescein (FAM). T7 RNA polymerase was incubated with the PCR products in the presence of 200 μ M I24 and initiator GTP before performing digestion with DNase I. Digested products were then analysed by capillary electrophoresis [26]. Clear protection of the T7 promoter in the presence of the T7 RNA polymerase initiation complex was observed (Figure 2B, left panels). However, in the presence of 200 μ M I24, no protection of the T7 promoter could be seen, indicating that the binding of the T7 RNA polymerase is impaired by the peptide. Interestingly, no protected sites were seen with the peptide alone in the absence of T7 RNA polymerase, indicating that direct interaction of the peptide with the DNA is not sufficient to protect the DNA from digestion by the DNase I.



Figure 1. Sequences of the 9-mer peptide I24, the TAT (48–60) peptide and the fusion peptide TAT-I24, synthesised as linear peptides.

The binding of the T7 RNA polymerase to the promoter leads to a transcription-competent open complex which forms a transcription bubble by melting of the DNA strands [25,27]. The open complex is then accessible to single-stranded specific chemical probes such as potassium permanganate (KMnO_4) leading to selective oxidation of single-stranded thymines which are not recognised by a DNA polymerase. Synthesis of the complementary strand is therefore terminated at the oxidised thymines. By KMnO_4 footprinting, an open complex by T7 RNA polymerase was observed in the presence of GTP/ATP/CTP. Interestingly, in this setting, I24 was unable to prevent strand separation at the promoter, indicating that I24 may affect the efficiency of T7 polymerase binding to DNA (Figure 2B, right panels).

To study the binding of I24 to the T7 promoter, a double-stranded oligonucleotide representing the T7 promoter was end-labelled with biotin and immobilised on streptavidin-coated sensor chips for binding analysis by surface plasmon resonance (SPR). Due to a predicted low solubility of the peptide in aqueous buffers, binding was performed in the presence of 5% DMSO. As shown in Figure 2C, I24 binds to the oligonucleotide representing the T7 promoter with an affinity of $K_D = 15$ nM.

2.2. The Fusion of Peptide I24 to the TAT Peptide Binds Double-Stranded DNA with High Affinity

Earlier data have shown that coupling of I24 to a cationic peptide, such as the TAT peptide (residues 48–60) from the HIV-1 transactivator protein (Figure 1), can strongly enhance the inhibitory effect of I24 on gene expression from a eukaryotic expression plasmid transfected with the peptide into cells. Moreover, coupling of I24 to TAT (TAT-I24; Figure 1) not only affected transfected DNA but also exerted a broad-spectrum antiviral activity against several double-stranded DNA viruses, including herpes simplex viruses, cytomegalovirus, vaccinia virus, adenovirus type 5 and SV 40 polyomavirus, an effect which was not seen with I24 alone [23]. It was, therefore, speculated that the TAT peptide contributes to the antiviral effects of the fusion peptide.

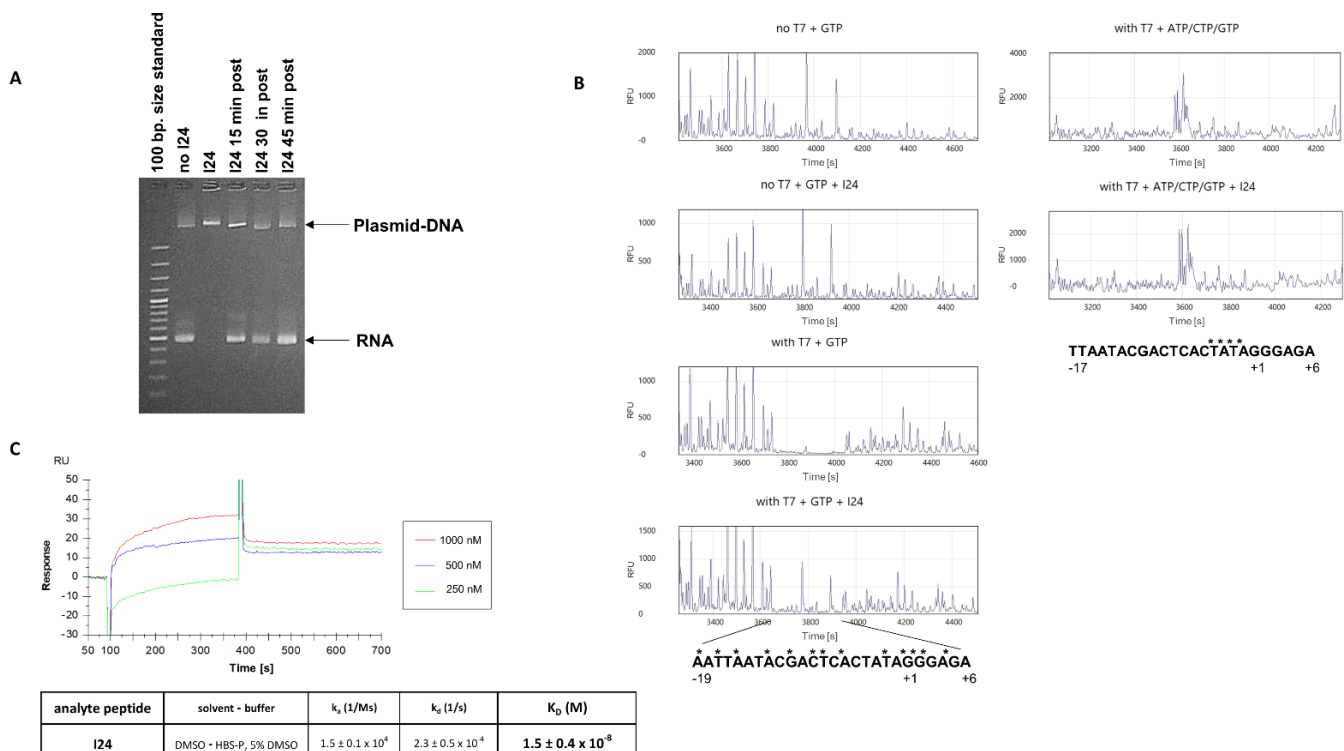


Figure 2. (A) In vitro RNA synthesis from a plasmid-DNA in the absence or presence of I24 (200 μ M) applied either simultaneously, or after 15, 30 and 45 min after initiation of RNA synthesis. (B) formation of T7 RNA polymerase initiation complex is inhibited by 200 μ M I24. Electropherograms from the reactions are shown. The y-axis shows the fluorescence intensity and the x-axis the elution position by time which corresponds to the size of the fragment. Asterisks above the sequence of the T7 promoter indicate bases protected from DNase I digestion by T7 RNA polymerase on the non-template strand (left panels). KMnO₄ footprinting in the absence and presence of 200 μ M I24 of the non-template strand with the formation of the open complex not inhibited by the peptide. Electropherograms from the reactions are shown (right panels). Asterisks above the sequence of the T7 promoter indicate KMnO₄-sensitive sites. Bases are numbered according to their position relative to the transcription start site. (C) SPR analysis of binding of I24 to a double-stranded oligonucleotide representing the T7 promoter performed in the presence of 5% DMSO. The calculated dissociation constant (K_D [M]) is shown.

The TAT peptide is a well-known cell-penetrating peptide [28,29]. It has been reported to bind to various molecules including double-stranded DNA with high affinity [30,31]. With increasing concentrations, the TAT peptide has been reported to cause a mobility shift of plasmid-DNA due to alterations of the net charge of the complex [30]. Agarose gel electrophoresis of plasmid-DNA incubated with increasing concentrations of TAT (48-60) peptide confirmed its binding to double-stranded DNA thereby causing an electrophoretic mobility shift and decrease in fluorescence intensity of ethidium bromide-stained plasmid-DNA (Figure 3A). This is in line with the reported fluorescence decrease after condensation of DNA with polycations [30,31]. However, in the presence of TAT-I24, the fluorescence of ethidium bromide-stained DNA was markedly reduced at concentrations above 1.3 μ M TAT-I24 indicating fluorescence quenching or displacement of the intercalating dye by the peptide (Figure 3A).

Fluorescence measurement using SYBR[®] Gold stain further confirmed the results obtained with agarose gel electrophoresis. Circular plasmid-DNA was incubated with increasing concentrations of TAT or TAT-I24 and stained with SYBR[®] Gold. While the TAT peptide caused a dose-dependent partial reduction of fluorescence intensity, TAT-I24 more potently reduced fluorescence to background levels (Figure 3B). In contrast, the peptide I24, lacking the TAT fusion partner, reduced fluorescence only to a low extent at concentrations up to 200 μ M (Figure 3C).

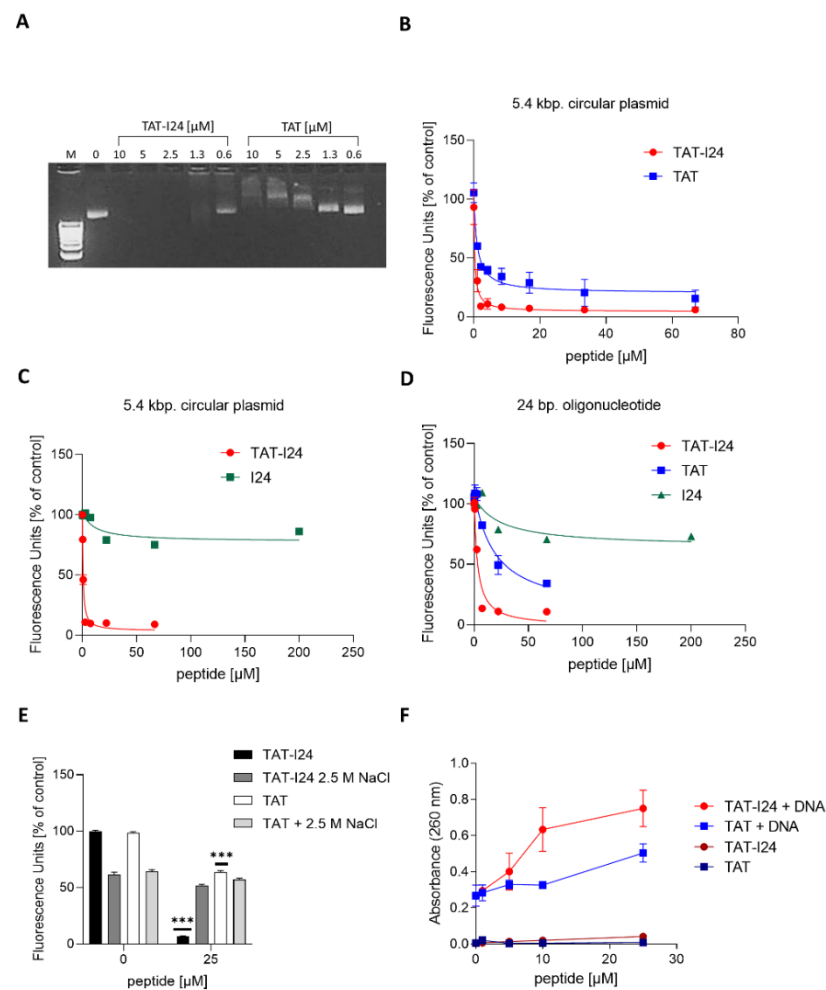


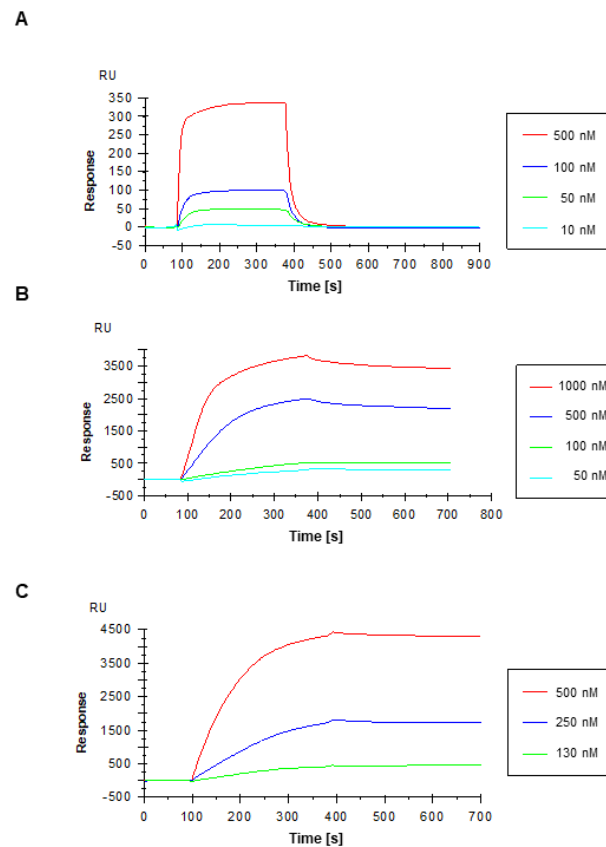
Figure 3. (A) Agarose gel electrophoresis of a plasmid-DNA incubated with increasing concentrations of TAT or TAT-I24 and stained with ethidium bromide, M = 1 kb. DNA ladder. (B) Fluorescence reduction of a 5.4 kbp. plasmid-DNA (pcDNA3.1) stained with SYBR[®] Gold stain and incubated with increasing concentrations of TAT or TAT-I24 performed in triplicate analysis and (C) incubated with TAT-I24 or I24 performed in duplicate analysis. (D) Fluorescence reduction of a 24 bp. double-stranded oligonucleotide (PC) stained with SYBR[®] Gold stain by increasing concentrations of I24, TAT or TAT-I24 performed in duplicate analysis. (E), Fluorescence reduction of an SYBR[®] Gold-stained plasmid-DNA in the absence or presence of 2.5 M NaCl performed in duplicate analysis. Multiple t-tests were performed for statistical analysis (***p* ≤ 0.001). (F) The absorbance of a plasmid-DNA at 260 nm in the presence of increasing concentrations of TAT or TAT-I24 performed in duplicate analysis.

Fluorescence was not only reduced from a plasmid-DNA but also from a short double-stranded 24 base pairs (bp.) oligonucleotide as used for SPR analysis (Figure 2C). The peptides TAT and TAT-I24 caused a reduction of fluorescence by SYBR[®] Gold stain, with TAT-I24 again being more effective in fluorescence reduction compared to the TAT peptide, while I24 caused only minor fluorescence reduction (Figure 3D). To analyse whether the DNA binding of TAT-I24 is sensitive to high concentrations of salt, which is known to affect protein-DNA interactions, fluorescence reduction by 25 μM TAT-I24 was tested in the presence of 2.5 M NaCl. While NaCl reduced fluorescence of untreated and TAT-bound DNA, the reduction caused by TAT-I24 could be restored with 2.5 M NaCl indicating that binding of the peptide is sensitive to salt (Figure 3E).

The binding of the TAT peptide to DNA has been shown to be associated with increased UV light absorbance at 260 nm. Hyperchromicity was observed with increasing concentrations of TAT peptide which is due to destabilization of the base pairs by the pep-

tide [32]. In the presence of TAT-I24, UV absorbance further increased indicating that the fusion peptide further enhances destabilization of the double-stranded DNA (Figure 3F).

Direct binding of TAT and TAT-I24 to the double-stranded DNA oligonucleotide as described above was further confirmed by SPR analysis. Although both peptides bound to the immobilised oligonucleotide, they displayed significantly different kinetic binding profiles in signal strengths (RU_{max}) as well as on- and off-rates. With a dissociation constant of $K_D = 75$ nM as opposed to $6.3 \mu\text{M}$ for the TAT peptide, TAT-I24 has approximately 100-fold higher affinity for binding to DNA compared to the TAT peptide, mainly due to a much lower off-rate (Figure 4A,B).



analyte peptide	solvent - buffer	k_a (1/Ms)	k_d (1/s)	K_D (M)
TAT	PBS - HBS-EP	$4.6 \pm 3.9 \times 10^3$	$2.6 \pm 1.6 \times 10^{-2}$	$6.3 \pm 2.3 \times 10^{-6}$
TAT-I24	PBS - HBS-EP	$5.4 \pm 0.8 \times 10^3$	$4.1 \pm 1.3 \times 10^{-4}$	$7.5 \pm 1.1 \times 10^{-8}$
TAT-I24	PBS - HBS-EP, 5% DMSO	$2.4 \pm 0.9 \times 10^4$	$3.8 \pm 2.2 \times 10^{-5}$	$2.0 \pm 1.6 \times 10^{-9}$

Figure 4. SPR analysis of peptides binding to a double-stranded oligonucleotide. The binding of TAT (A) and TAT-I24 (B) in the HBS-EP buffer is shown. (C) binding of TAT-I24 in the presence of 5% DMSO. Calculated dissociation constants (K_D [M]) are shown.

As the affinity of I24 in the presence of 5% DMSO was 15 nM, the binding of TAT-I24 was also tested under these conditions. The presence of DMSO further increased the binding affinity of TAT-I24 ($K_D = 2$ nM) as shown in Figure 4C. This increase in affinity in the presence of 5% DMSO could be explained by the oxidative effect of the solvent on the three cysteines in I24 presumably leading to stabilization of the binding.

2.3. TAT-I24 Blocks Activity of Taq DNA Polymerase from Double-Stranded DNA

DNase I footprinting experiments, as performed with I24 (Figure 2B), were also conducted with TAT-I24. However, in the presence of TAT-I24, the expected digestion patterns could not be observed indicating that the DNA is tightly bound by TAT-I24

making it insusceptible to limited DNase digestion. Therefore, a different approach was chosen to analyse the impact of TAT-I24 complexing with DNA. It was tested, whether the activity of a DNA polymerase, such as the heat-resistant Taq polymerase, can be also inhibited by DNA-bound TAT-I24. A circular plasmid (pCDNA3.1-luciferase) containing the luciferase coding region was incubated with increasing concentrations of TAT, TAT-I24 or I24 followed by ethanol-precipitation, washing and dissolving the samples before being subjected to real-time PCR. While the peptides I24 or TAT complexed with DNA did not markedly affect the PCR amplification, TAT-I24 clearly affected the efficiency of the PCR. At concentrations above 1 μM , TAT-I24 caused a prominent shift of the cycle threshold (CT) by > 15-PCR cycles (Figure 5A). To test if this effect is due to inhibition of polymerase binding caused by binding of TAT or TAT-I24 to DNA, a plasmid containing the luciferase coding region (pGL3-promoter) was incubated with 25 μM TAT-I24, ethanol-precipitated, dried and dissolved. The treated plasmid at 1, 5 and 10 \times molar excess was incubated with pCDNA3.1-luciferase. As pCDNA3.1-luciferase contains a neomycin resistance gene which is lacking in the pGL3-promoter plasmid, the neomycin gene was chosen as the target for amplification. Real-time PCR of the neomycin resistance gene showed that in the presence of equal amounts of treated and untreated plasmids, amplification of neomycin was not affected. Only at 5-fold and 10-fold excess of peptide-treated plasmid was the amplification of the neomycin reduced, as witnessed by a shift of CT values by about 2, indicating that the inhibitory action of TAT-I24 is associated with its binding to DNA and is not due to non-specific inhibition of the PCR reaction (Figure 5B).

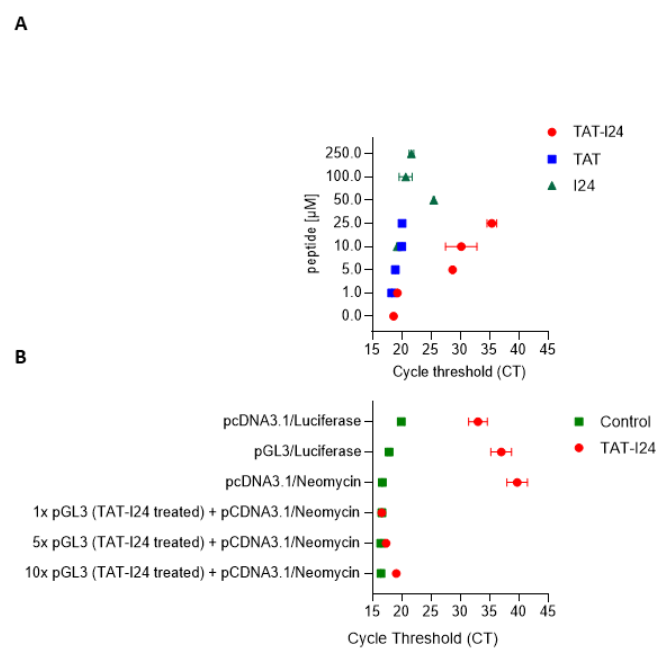


Figure 5. (A) Plasmid-DNA was incubated with increasing concentrations of TAT, TAT-I24 or I24, ethanol precipitated and subjected to real-time PCR detecting parts of the luciferase coding region. The shift of the cycle threshold (CT)-value indicates binding of TAT-I24 to the DNA and blocking of polymerase activity. (B) Plasmids were incubated with 25 μM TAT-I24, ethanol-precipitated and subjected directly to real-time PCR. Plasmid-bound TAT-I24 impacts amplification of luciferase from the pGL3-promoter plasmid (pGL3) or of luciferase and neomycin resistance gene (pcDNA3.1) by shifting the CT. Minor impact of excess of TAT-I24-bound and precipitated pGL3-promoter plasmid (pGL3; TAT-I24 treated) on amplification of neomycin resistance gene of an untreated plasmid (pcDNA3.1).

2.4. Fluorescence Measurement and Molecular Modelling of the Peptide-DNA Complexes

Two hairpin oligonucleotides with a short double-stranded AT or GC stretch (following Hsu et al., 2005) were used to study the binding of the peptides [33]. Reduction in

fluorescence by DNA-bound SYBR[®] Gold stain was observed with both oligonucleotides and the TAT peptide. The peptide TAT-I24 further decreased the fluorescence of both oligonucleotides (Figure 6A).

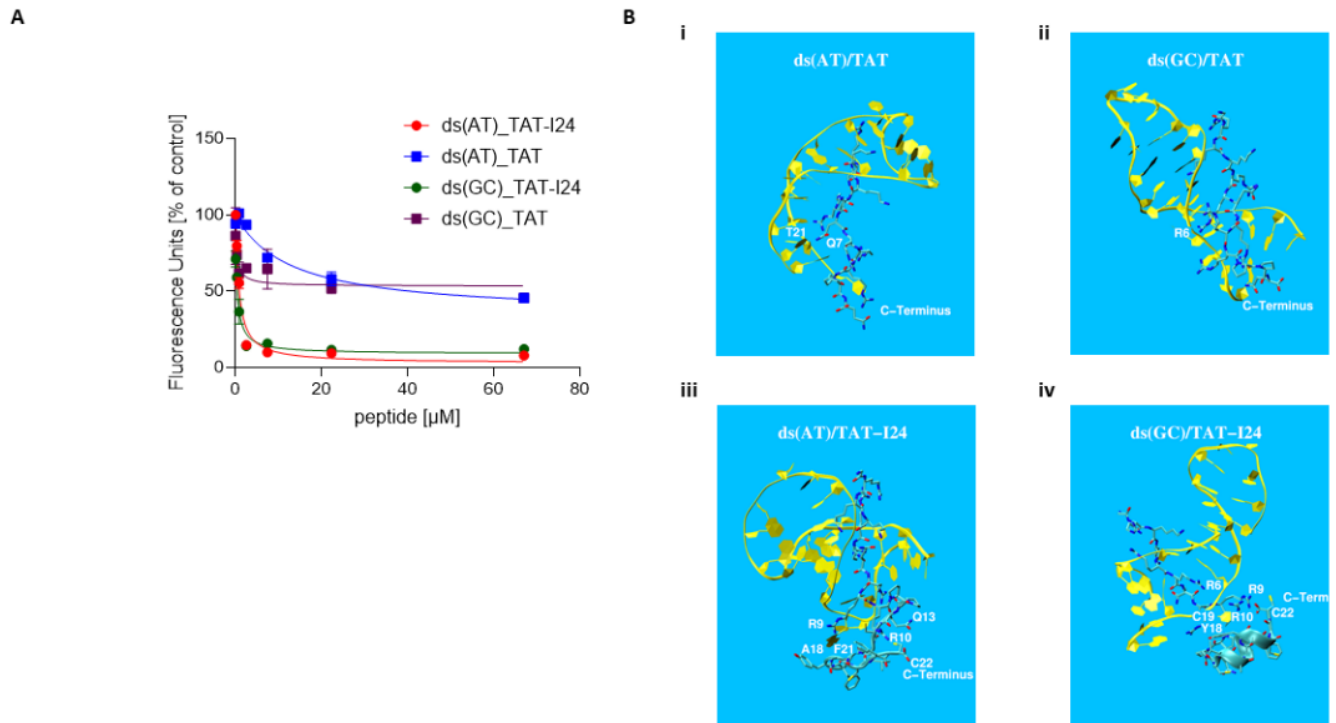


Figure 6. (A) Reduction of fluorescence by TAT or TAT-I24 bound to ds (AT) or ds (GC) hairpin oligonucleotides. (B) Structural snapshots obtained from MD simulations of TAT (i,ii) and TAT-I24 (iii,iv) complexed with the ds (AT) or ds (GC) hairpin oligonucleotides. A detailed description of key structural elements is provided in the main text.

Molecular dynamics simulations (MD) were carried out to study molecular modes of interaction of TAT and TAT-I24 to these hairpin oligonucleotides. The structural information could be derived from a crystal structure of the TAT protein in HIV-1 (pdb code 6CYT; [34]) that identifies its location in close proximity to the RNA stem-loop (see Figure S1a for the relative position of the N-terminal Gly coloured in green to the RNA indicated in yellow). A related NMR structure (pdb code 6MCE; [35]) provides detailed insight into molecular interactions between several positively charged lysine (K) and arginine (R) residues in TAT (indicated as the blue stretch in Figure S1b) and the backbone of the RNA (indicated in yellow in Figure S1b) facilitated mainly by the negatively charged phosphate groups of the nucleic acid. Consequently, 6MCE was taken as a template for systematic affinity studies of peptide/ds (AT/GC) complexes. Residues in the template structure were adopted to match the 4 complexes; TAT or TAT-I24 with ds (AT) or ds (GC). As an example, a structural snapshot of the assembled complex TAT-I24/ds (AT) is shown in Figure S2. All 4 complexes were embedded in explicit water and studied by long term MD simulations (250 ns, AMBER-18, pmemd.cuda, NpT, 300 K, 1 bar, $\Delta t = 1$ fs). The time evolution of these 4 MD simulations is shown in Video S1 dna-tat-md-250ns.mp4 (360° view). Remarkable structural elements are summarised in Figure 6B: in both complexes, TAT/ds (AT) and TAT/ds (GC), the N-terminal end shows minor molecular mobility when compared with the C-terminal end, which exhibits vigorous movements. Positively charged NH_i^+ groups at R/K residues try to adopt maximum distances relative to each other, thereby forming extensive interactions with negatively charged phosphate groups on the DNA backbone. While TAT/ds (GC) maintains classic Watson/Crick pairs over a sizeable range (nucleotides 5–9), most of the base pairs in TAT/ds (AT) are broken up (except AT pairs 3, 4 and 5). Some of the peptide residues in the TAT/ds (AT) complex substitute lost nucleotide bases,

for example, glutamine 7 (Q7) and thymine 21 (T₂₁), as shown in Figure 6Bi. Conversely, residue arginine 6 (R6) in the TAT/ds (GC) complex is finger-pointing at GC pair number 4 thereby breaking it open (Figure 6Bii). In contrast to the TAT-only complexes, both TAT-I24 complexes show significant stabilization of the C-terminus. In TAT-I24/ds (AT) the C-terminal helix unfolds and forms a loop where the COO⁻ group of cysteine (C) 22 gets stabilised by R10 and Q13, the former also chelating phenylalanine (F) 21 with the help of R9. This re-arrangement significantly enhances structural stability and forms solid support for adjacent nucleotides, e.g., alanine (A) 18 (see Figure 6Biii and supplementary Video S1 “dna-tat-md-250ns.mp4”). Practically all classic Watson/Crick pairs are lost. TAT-I24/ds (GC) displays strong levels of intra-peptidic stabilization of the COO⁻ group by R9 and R10 with the helical element perfectly conserved. This also provides support for adjacent nucleotides, e.g., tyrosine (Y)18-cytidine 19 (C₁₉). Despite residue R6 displacing the 3rd and 4th Watson/Crick pair, the rest of the GC pairs remain well established over the entire simulation time (see Figure 6Biv and supplementary Video S1 “dna-tat-md-250ns.mp4”).

Quantification of the strength of binding of the peptides to hairpin DNAs was assessed with the help of MM/PBSA calculations [36,37]. This type of assessment plays a critical role in biomedical/physiological research with ongoing efforts in extending the method towards more complex, biologically relevant environments, e.g., biomembranes [38–40]. Results of the 4 complexes studied are summarised in Table S1. Due to the significant structural re-arrangement occurring in the initial stage of the underlying MD simulations, a variety of truncated evaluation periods have been taken into account ranging from the entire 250 ns down to considering just the final 50 ns (where the complex is assumed not to undergo any further structural alterations). Both major methods of treating continuum electrostatics, GB and PB, were applied and entropic contributions added optionally (values given in parentheses in Table S1). When focusing on the final section of MD trajectories, binding free energies may be ranked as $\Delta G_{ds(GC)/TAT-I24} < \Delta G_{ds(AT)/TAT-I24} < \Delta G_{ds(GC)/TAT} < \Delta G_{ds(AT)/TAT}$. Hence the highest affinity is determined between peptide TAT-I24 and hairpin DNA formed of ds (GC).

2.5. Effect of TAT-I24 on Viral DNA Upon Entry

Earlier data indicated that entry of murine cytomegalovirus (MCMV) is affected by TAT-I24, visualised by a virus containing an mCherry-labelled capsid [23]. To address any possible interaction of the peptide TAT-I24 with the viral DNA, cells were infected with a bromodeoxyuridine (BrdU)-labelled MCMV expressing luciferase [41]. Fixation of cells after virus adsorption at 4 °C showed a clear, punctate pattern of BrdU-labelled viral DNA. However, in the presence of TAT-I24 and compared to the untreated control, the number of foci was reduced already during adsorption and remained low after 15 and 60 min, supporting earlier observations with the mCherry-labelled virus (Figure 7A).

To distinguish between a potential effect on viral entry or a direct effect of TAT-I24 on the viral DNA, cells were infected with BrdU-labelled virus and after one hour, fixed and permeabilised. Then, 10 µM TAT-I24 was added to fixed cells and incubated for another hour. Cells were then washed, DNA denatured by treatment with HCl and stained with the BrdU-antibody. Interestingly, almost no signal could be detected in cells treated with TAT-I24 after fixation and permeabilization, indicating that TAT-I24 interacts with the DNA in such a way that binding of the antibody is inhibited (Figure 7A).

The BrdU-labelled virus was adsorbed to NIH/3T3 cells in the presence of fluorescein-conjugated TAT-I24 (FAM-TAT-I24) at 4 °C for 1.5 h. The FAM-labelled peptide has been reported by us previously to be predominantly membrane-localised [23]. After adsorption, the unbound virus was removed by washing and the cells incubated at 37 °C for 30 min. before fixation and staining with the BrdU-antibody. Microscopic examination showed foci of BrdU-labelled DNA in the red fluorescence channel as well as cytosolic foci of green fluorescence derived from the FAM-labelled peptide. At high contrast settings of the blue fluorescence, BrdU signal co-localised with DAPI which stains the viral DNA (Figure 7B).

In several cases, juxtaposition and co-localization of the signals in all three channels were observed, indicating close vicinity and binding of the peptide to the viral DNA (Figure 7B).

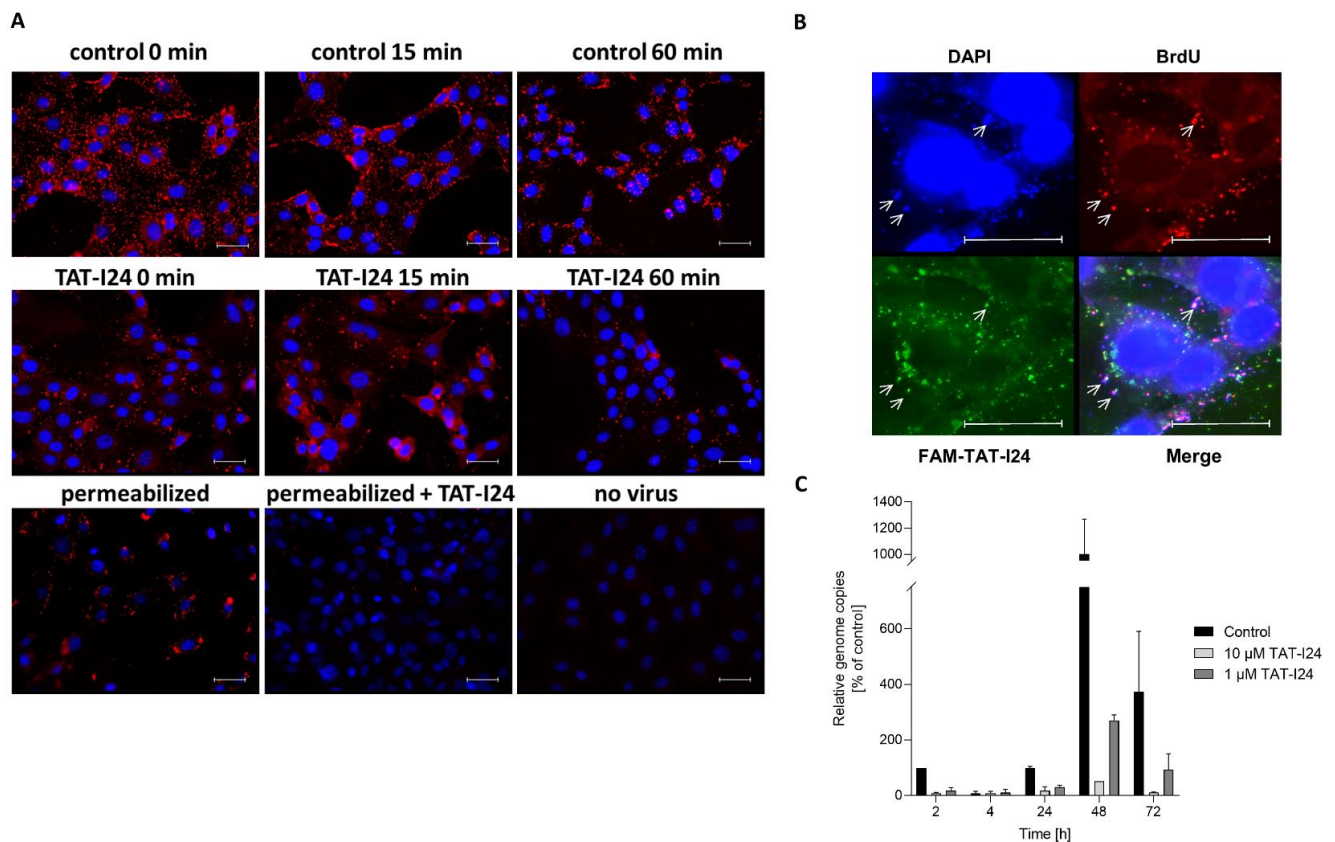


Figure 7. (A) Localisation of BrdU-labelled MCMV-luc DNA genomes after infection (MOI 0.25) in the absence or presence of 10 μ M TAT-I24 before cold-release (0 min) or 15 and 60 min post-cold release. After fixation, cells were permeabilised and stained with the BrdU antibody (upper and middle panel). In addition, cells were infected and left untreated for 120 min, fixed and permeabilised. Then, permeabilised cells were treated with medium alone or with medium and 10 μ M TAT-I24, washed and stained with the BrdU antibody (lower panel). (B) Co-localization of BrdU-labelled MCMV-luciferase DNA and FAM-labelled TAT-I24 30 min post-cold release. Arrows indicate juxtaposition and co-localisation of blue fluorescence (DAPI) at high contrast settings, green fluorescence (FAM-TAT-I24) and BrdU-labelled viral DNA (red fluorescence). Nuclei are visible with DAPI (40 \times objective); scale bars indicate 40 μ m. (C) MCMV-luciferase was adsorbed with the aid of centrifugal enhancement to NIH/3T3 cells and cells were washed before temperature shift to +37 $^{\circ}$ C. Total DNA was isolated from cells at the indicated time-points after cold release and viral DNA quantified by real-time PCR detecting luciferase and normalised to 18S rDNA. Relative DNA levels expressed as % of control (2 h, unstimulated control is set as 100%) is shown. Data shown are mean \pm SD from two independent experiments.

For this reason, levels of viral DNA were also analysed by quantitative real-time PCR. NIH/3T3 cells were infected with MCMV expressing luciferase and viral DNA isolated after 2, 4, 24, 48 and 72 h. Relative viral genome copies were determined by real-time PCR using the detection of firefly luciferase encoded in the viral genome. After 2 h, an approximately 10-fold decrease in viral genome copies was observed in the presence of 1 and 10 μ M TAT-I24. However, after 4 h, overall viral DNA was also reduced in the control group. Based on the observation that TAT-I24 complexed with DNA could affect the efficiency of the PCR (Figure 5), it is likely that the peptide bound to the viral genome also affects PCR efficiency, leading to a shift in CT value. After 24 h, DNA levels started to increase in the control group, while after 48 h, active viral DNA replication is evident but to a lesser extent in TAT-I24-treated cells. After 72 h, DNA synthesis declines, with DNA levels remaining slightly above background when infection was performed in the presence of 10 μ M TAT-I24 (Figure 7C).

2.6. Inhibitory Effect of TAT-I24 Is Prevented by Preincubation of the Peptide with Double-Stranded DNA

Based on the notion that TAT-I24 can bind DNA with high affinity, we examined the effect of saturation of the peptide with double-stranded DNA on its antiviral activity. COS-7 cells were incubated with increasing concentrations of TAT-I24 in the presence of salmon sperm DNA (1 mg/mL). Cells were then transduced with baculovirus-luciferase which expresses the reporter gene luciferase under the control of the CMV promoter [23]. While luciferase expression was dose-dependently inhibited by TAT-I24, no reduction of its expression was seen when the peptide was saturated with DNA before addition to the cells. These data indicate that the binding of TAT-I24 to excess amounts of DNA blocks its antiviral activity and that the same sites of the peptide are involved in both DNA binding and antiviral activity (Figure 8A).

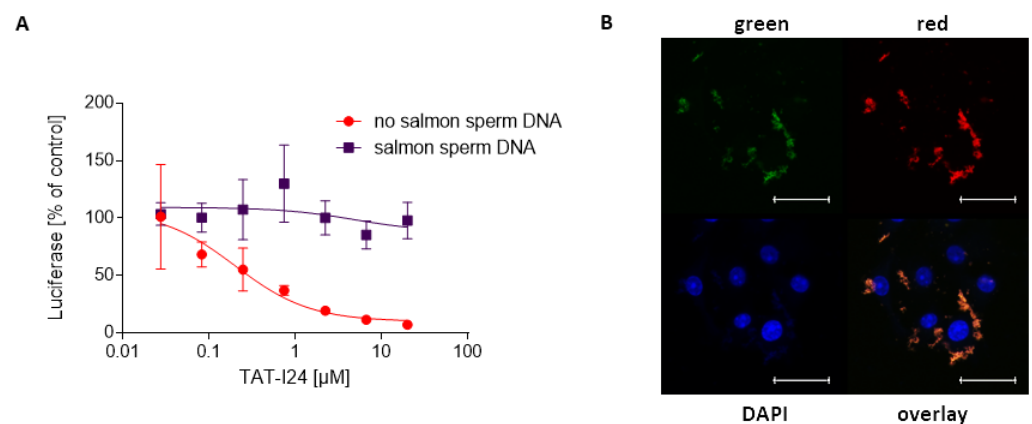


Figure 8. (A) COS-7 cells were treated with increasing concentrations of TAT-I24 either alone or in the presence of 1 mg/mL salmon sperm DNA and subsequently infected with Baculovirus-Luc. Cells were lysed after 24 h and subjected to luciferase analysis. The results shown are mean \pm SD from triplicate wells. (B) COS-7 cells were treated with 20 μ M TAT-I24 in the presence of salmon sperm DNA and stained with DAPI. Microscopic examination (40 \times objective) in the channels blue (DAPI), green and red. An overlay of all channels indicates aggregates of DNA and peptide located at the cell surface with fluorescence emission in the green and red channel. Scale bar indicates 40 μ m.

To determine whether the peptide can bind to the cell surface in the presence of salmon sperm DNA, COS-7 cells were treated with 20 μ M TAT-I24 and salmon sperm DNA (1 mg/mL), fixed and stained with DAPI. Apart from the known staining of the chromosomal DNA by DAPI, aggregates at the cell surface were also stained, indicating that TAT-I24 forms large complexes with DNA which are also localised at the cellular membrane. Further microscopic analysis in other fluorescence channels of the microscope showed that the DNA-peptide complex emitted fluorescence in the green and red channels (Figure 8B). No fluorescence was recorded when TAT-I24 was applied to the cells in the absence of salmon sperm DNA alone or with TAT peptide in the presence of salmon sperm DNA (Figure S3).

3. Discussion

We have previously reported that the peptide TAT-I24, a fusion of the 9-mer peptide I24 and the TAT peptide, can neutralize a broad range of DNA viruses, including herpes simplex virus, cytomegalovirus, vaccinia virus, polyomavirus and adenovirus without cytotoxicity at the concentrations used. The model suggested that the peptide bound to the cell membrane could reduce viral entry but can also be internalised together with the virus where it exerts its inhibitory effect by binding to the viral DNA upon uncoating [23]. To further support this model, the present study aimed to investigate the DNA-binding properties of the TAT-I24 fusion peptide.

The TAT peptide is a well-known cell-penetrating peptide [28,29] that has been shown to strongly interact with DNA and can promote the entry of DNA into cells [30,31]. Due to its cell-penetrating properties and ability to bind and condense DNA, the TAT peptide has been evaluated as a gene delivery agent [42]. However, in contrast to the TAT peptide itself, TAT-I24 does not enhance gene transfer but rather inhibits gene expression from the "foreign" DNA. This inhibitory feature is provided by I24, which can block gene expression from a transfected plasmid-DNA as well as RNA transcription and binding of T7 RNA polymerase to a DNA template. However, although I24 alone can inhibit gene expression when complexed with the DNA in the transfection reaction, it is not sufficient to inhibit infection with a virus, indicating that the peptide may not reach the site of action where it could exert this activity [23].

The TAT peptide itself has been reported to inhibit herpes simplex virus infections, an effect which is enhanced by the addition of a C-terminal cysteine [43,44]. However, while minor or no effect was seen from the TAT peptide in various infection models, the fusion of I24 to the TAT peptide, as in TAT-I24, neutralised several different types of viruses [23]. It is therefore likely that the TAT fusion partner is required to guide I24 to the cell membrane. Additionally, the TAT fusion partner further enhanced the potency of the peptide in the transfection system [23]. The different effects of the peptides observed in cell culture models are also reflected by their binding to DNA in the present study. The peptide TAT-I24 exhibited an approximate 100-fold enhanced affinity for DNA compared to the TAT peptide, due to different binding kinetics of TAT-I24 compared to the TAT peptide with a much lower off-rate. The binding of TAT or TAT-I24 to double-stranded DNA could be further visualised by levels of fluorescence from DNA-intercalating dyes such as ethidium bromide or SYBR[®] Gold stain, with TAT-I24 reducing fluorescence. This adds support to the idea that once DNA is bound by the peptide TAT-I24, subsequent steps such as polymerase binding are substantially inhibited. This model is further supported by the observation that TAT and TAT-I24 may destabilize DNA, which is also predicted by molecular modelling. However, it is also possible that after endocytosis of TAT-I24, the peptide remains trapped in the endosome together with its cargo, the viral DNA, and is targeted to the lysosome or redistributed to the membrane, a phenomenon reported occurring with many cell-penetrating peptides [45,46].

The remaining question relates to which features of the peptide contribute to the high binding affinity. Molecular dynamics simulation together with MM/PBSA calculations [37] of the DNA-bound peptide provides a model of binding of TAT-I24 to DNA duplexes involving arginine residues from the TAT fusion partner together with residues A16, Y18, F21 and C22 of I24. The most obvious feature identified is the silencing of molecular motion occurring at the C-terminus (see Video S1 dna-tat-md-250ns.mp4). This can increase the tightness of coupling between the peptide and the DNA. The length and amino acid composition of TAT-I24 are perfectly chosen to exactly fit into the major groove of the DNA backbone. There is a clear increase in binding affinity when switching from ds (AT) to ds (GC) DNA both for the bare TAT peptide as well as for TAT-I24. This may simply reflect the well-known stability enhancement in DNA with growing GC-content. On the molecular level, this could indicate a requirement for a rather rigid binding matrix because of the rather strong Coulombic interaction occurring between negatively charged phosphate groups on the DNA backbone and the positively charged NH_3^+ groups on R/K residues. However, the effect should still be regarded as sequence-unspecific binding enhancement with a potential role in boosting the efficacy of antimicrobial peptides [36].

One obvious feature of I24 is the presence of three cysteine residues which are assumed to stabilize the binding. DNA complexing and gene transfer by the TAT peptide has been shown to be enhanced by additional histidine and cysteine residues through stabilizing the DNA-binding via interpeptide disulphide bonds [47,48]. Of note, defensins are cationic peptides containing several cysteines which are pivotal for full activity [49]. Apart from binding to surface molecules, binding to the viral DNA has also been suggested to contribute to the antiviral activity of some defensins. Such binding has been reported for

the human defensins HNP-2 and HD-5, determined by fluorescence quenching of ethidium bromide-stained DNA [50]. It is possible, and likely, that TAT-I24 exerts similar activity as some defensins.

It is currently not clear how the peptide could contact the viral genome during infection, as the viral DNA is protected from the environment by the viral capsid and is released only in the infected cell during the process of uncoating. A possible mechanism of inhibition could be an effect on endosomal acidification itself due to the presence of several basic amino-acid residues, as reported for the defensin-derived peptide P9R which can inhibit infection with coronaviruses, influenza virus and rhinovirus [9,51]. However, extraction and quantification of viral DNA showed that, in cells infected with the same amount of virus but treated with TAT-I24, viral DNA is apparently reduced by 90% compared to untreated controls, already after two hours. Since at this stage *de novo* DNA synthesis is not possible, this shift can only be explained by an effect of the peptide after virus entry and by complexing of the viral DNA with TAT-I24 and consequently, inhibition of transcription. Further evidence for the connection between DNA-binding and antiviral effect is that the antiviral activity is lost when the peptide is preincubated with unrelated DNA. Furthermore, reduction of BrdU-labelled viral DNA after post-cold release could suggest inhibition of virus entry, but could also be caused by the blocking of antibody binding to DNA by TAT-I24 which was observed when the peptide was added after fixation of infected cells. Additional evidence for a direct effect of the peptide on the viral DNA comes from the observed juxtaposition and co-localization of BrdU-labelled DNA and FAM-labelled peptide, indicating a close vicinity of peptide and DNA. Further imaging procedures using electron microscopy and are required to determine the exact localization of the peptide during infection and binding to the viral genome.

Preliminary data also indicate that the binding is not restricted to double-stranded DNA, as binding of TAT-I24 to single-stranded DNA and RNA could also be observed. However, more investigations are required to characterize binding to RNA and are the subject of ongoing studies.

Taken together, our study demonstrates that the antiviral peptide TAT-I24 can bind double-stranded DNA with high affinity and we provide evidence that this binding is indispensable for the antiviral effect. Further modifications are currently being generated to address nucleic-acid binding affinity of the peptide and the selective inhibition of viral gene expression without affecting host cell gene expression. This is of particular importance to exclude any cytotoxicity associated with the DNA-binding of the peptide.

4. Materials and Methods

4.1. Peptides

Peptides were synthesised at JPT Peptide Technologies (Berlin, Germany) or Bachem AG (Bubendorf, Switzerland). The peptides CLAFYACFC (I24), GRKKRRQRRRPPQ-CLAFYACFC (TAT-I24) or GRKKRRQRRRPPQ (TAT 48-60) were purified with HPLC to >90% purity. The peptide FAM-TAT-I24 consisting of a fusion of TAT (4757) and I24 labelled with 6-carboxyfluorescein at the N-terminal end was synthesised at Bachem AG (Bubendorf, Switzerland) and has been described previously [23]. All peptides were obtained freeze-dried and subsequently dissolved in DMSO (Sigma-Aldrich, Schnelldorf, Germany) or PBS as 10 mM stock and stored at -20°C .

4.2. Plasmids

A 465 bp. DNA fragment was cloned into the EcoRI and BstEII sites of pCDNA3.1 (pcDNA3.1-VEGF). The pGL3-promoter plasmid was obtained from Promega (Mannheim, Germany) and pcDNA3.1 (+) from ThermoFisher (Darmstadt, Germany). The plasmid pcDNA3.1-luciferase was described previously [23]. All plasmids were purified from *E. coli* cultures using Wizard[®] Plus Midiprep DNA Purification System (Promega, Mannheim, Germany).

4.3. RNA Synthesis and Binding of T7 RNA Polymerase

The plasmid pcDNA3.1-VEGF was linearised with BstEII and used as a template for transcription by T7 RNA polymerase using the RiboMAX Large Scale RNA Production System-T7 (Promega; Mannheim, Germany), leading to the synthesis of an RNA of 465 bases in size. RNA synthesis was performed in a 10 µL reaction with 100 ng of linearised plasmid-DNA for 60 min at 30 °C. The peptide was added either simultaneously or after 15, 30 and 45 min of synthesis. Five µL of the reactions were loaded per lane of an agarose gel and stained with SYBR™ Gold Nucleic Acid Gel Stain (ThermoFisher, Darmstadt, Germany).

All oligonucleotides in this study were synthesised at Microsynth AG (Balgach, Switzerland). DNase I footprinting was performed using a 359 bp. double-stranded DNA fragment generated by PCR from pcDNA3.1-VEGF using FAM-labelled pcDNA3.1 forward primer: 5'-FAM-TAACAACTCCGCCCCATTGA-3' and VEGF reverse primer: 5'-TCCACCAGGGTCTCGATTGG-3'. A mixture containing transcription buffer, PCR product and GTP was incubated with or without T7 polymerase in the absence or presence of 200 µM I24 for 5 min at 37 °C followed by the addition of 16 ng human genomic DNA, 1 µL 100 mM CaCl₂ and 1 µL of DNase I (Qiagen, Hilden, Germany) 1:1000 diluted in DNA digestion buffer. Reactions were incubated at room temperature and stopped after 4 min. by addition of 0.5 µL 25 mM EDTA. DNA fragments were purified using QIAquick PCR Purification Kit (Qiagen, Hilden, Germany). Fragments were then analysed using an ABI PRISM® 310 Genetic Analyzer and a GeneScan™ 500 ROX™ dye Size Standard (ThermoFisher, Darmstadt, Germany).

KMnO₄ footprinting was performed according to published protocols with modifications [52,53]. A 359 bp. PCR fragment was generated by PCR from pcDNA3.1-VEGF with unlabelled pcDNA3.1 forward and VEGF reverse primer. A mixture containing transcription buffer, PCR product and GTP/ATP/CTP was incubated with or without T7 polymerase in the absence or presence of 200 µM I24 for 15 min at 30 °C, followed by the addition of 10 µL 10 mM KMnO₄ for 3 min at 30 °C. The reaction was then stopped by the addition of 2.4 µL b-mercaptoethanol and placed on ice. After the addition of 2.6 µL 0.5 M EDTA, DNA was purified by phenol-chloroform extraction and precipitation by addition of 1/10 of the volume 3 M sodium acetate and 2.5× volumes of 96% ethanol, spinning for 20 min at maximum speed in a microcentrifuge and then washing with 80% ethanol followed by air drying of the pellet. DNA was then dissolved in 10 µL water and subjected to a primer extension assay with AmpliTaq Gold polymerase and 25 cycles of asymmetric PCR using FAM-labelled pcDNA3.1 for primer 5'-FAM-TAACAACTCCGCCCCATTGA-3'. After that, the reaction was again subjected to phenol-chloroform extraction and ethanol precipitation before analysis of fragments using an ABI PRISM® 310 Genetic Analyzer and a GeneScan™ 500 ROX™ dye Size Standard (ThermoFisher, Darmstadt, Germany). Calculation of DNase I-protected sites or KMnO₄-sensitive sites was performed using Peak Scanner Software 2 (ThermoFisher, Darmstadt, Germany) and Osiris (National Center for Biotechnology Information, Bethesda, MD, USA).

4.4. DNA Gel Retardation Assay

100 ng circular plasmid-DNA (pcDNA3.1-Luc) was incubated with increasing concentrations of the peptide TAT-I24 for 10 min. at room temperature in a volume of 20 µL H₂O. Plasmids were then ethanol-precipitated, washed, air-dried and dissolved in 10 µL water and loaded on a 1.4% agarose gel. Electrophoresis was performed in TAE buffer in the presence of ethidium bromide (0.25 µg/mL).

4.5. Fluorescence Measurements

The circular pcDNA3.1 (+) plasmid (100 ng) was incubated with increasing concentrations of peptides in 50 µL TE buffer in black 96-well plates. After 5 min, 5 µL of SYBR® Gold stain (ThermoFisher, Darmstadt, Germany) was added (1:400 diluted from concentrate). For high-salt treatment, 55 µL of 5 M NaCl were added to the wells. In all

measurements, fluorescence was recorded after 5 min using the GloMax[®]-Multi Detection System (Promega, Mannheim, Germany) using the optical kit blue (excitation wavelength 490 nm, emission wavelength 510–570nm). For analysis of peptide-binding to double-stranded DNA oligonucleotides, the following oligonucleotides were used: PC_for: 5'-GAAATTAATACGACTCACTATAGGG-3' and PC_rev: 5'-CCCTATAGTGAGTCGTATTAATTT-3'. The oligonucleotides were mixed at equimolar concentrations, heated to 95 °C and annealed by slow cooling for approximately two hours to room temperature. Hairpin oligonucleotides used in this study were ds (AT): 5'-CATATATATCCCCCATATATATG-3' and ds (GC): 5'-CGCGCGCGTTTTCGCGCGCG-3' according to Hsu et al. [33] with the loop region underlined. Hairpin oligonucleotides were dissolved at a concentration of 12 µM, heated to 95 °C followed by slow cooling for approximately two hours to room temperature.

4.6. UV Radiation

Increasing concentrations of TAT or TAT-I24 were incubated with pcDNA3.1 plasmid-DNA (1.5 µg) in 100 µL TE buffer (10 mM Tris/HCl, pH 8.0, 1 mM EDTA) and UV absorbance at 260 nm determined using a Biophotometer (Eppendorf, Hamburg, Germany) and compared to absorbance by peptides in the absence of DNA.

4.7. Surface Plasmon Resonance

A double-stranded oligonucleotide was generated by annealing of the biotinylated oligonucleotide PC_for: 5'-biotin-GAAATTAATACGACTCACTATAGGG-3' and PC-rev. Annealing of the oligonucleotides was performed as described above. The double-stranded oligonucleotide was then immobilised on a streptavidin-coated Biacore SA sensor chip at varying ligand surface densities. The peptides TAT or TAT-I24, both dissolved in phosphate-buffered saline (PBS) as 10 mM stock, were diluted with HEPES-buffered saline (HBS) to concentrations of 1 µM to 0.01 µM for determination of binding kinetics. The binding of the peptide I24 and TAT-I24, both dissolved as 10 mM stock in DMSO, was also analysed in the presence of 5% DMSO. Binding was determined using a Biacore[™] 3000 Instrument (Biacore, Cytiva, Marlborough, MA, USA). Kinetic constants and affinities were generated with different dilutions of the peptides, which had been chosen from pilot experiments to provide optimal sensorgram running conditions. Kinetic binding constants were calculated from the fitted curves using a simultaneous global fitting process applying a Langmuir 1:1 binding algorithm (BiaEvaluation 4.1 software, Cytiva, Marlborough, MA, USA).

4.8. Plasmid-DNA Binding Assay

For DNA-binding assays, circular plasmids (100 ng) were incubated with 25 µM TAT-I24 in a 20 µL reaction for 10 min followed by ethanol-precipitation as described above. Pellets were washed once with 50 µL of 70% ethanol, air-dried and dissolved in 20 µL of water. For use in real-time PCR, samples were diluted 1:100 in water and 1 µL (50 pg plasmid) was used per real-time PCR reaction. Real-time PCR for detection of luciferase was performed using the primers luciferase for 5'-TGGAGAGCAACTGCATAAGG-3' (600 nM), luciferase rev: 5'-CGTTTCATAGCTTCTGCCAA-3' (600 nM), the luciferase probe: 5'-FAM-ACGCCCTGGTTCCTGGAACAA-TAMRA-3' (200 nM) and for detection of the neomycin resistance gene neomycin for 5'-GGAGAGGCTATTCGGCTATG-3' (600 nM), neomycin rev: 5'-GACAGGTCGGTCTTGACAAA-3' (600 nM) and neomycin probe: 5'-FAM-CTGCTCTGATGCCGCCGTGT-TAMRA-3' (200 nM) and TaqMan[™] Fast Universal PCR Master Mix (ThermoFisher, Darmstadt, Germany). PCR was performed using an Applied Biosystems[®] 7500 Fast Real-Time PCR System (ThermoFisher, Darmstadt, Germany).

4.9. Cell Culture

COS-7 and NIH/3T3 cells were adapted to growth in CO₂-independent medium supplemented with 10% fetal calf serum, 2 mM glutamine and 1% antibiotic-antimycotic (ThermoFisher, Darmstadt, Germany) and cultivated in a humidified atmosphere at 37 °C and passaged once a week. For peptide treatments, DMSO concentrations in the experi-

ments were not exceeding 0.2%. At this concentration, no toxic effects on the cells were seen in our previous studies [23].

4.10. Baculovirus

A baculovirus expressing luciferase under the control of the CMV promoter has been described previously [23]. COS-7 cells were seeded at a density of 2.5×10^4 cells/well in 96-well plates. On the next day, cells were treated with dilution series of TAT-I24 either alone or in the presence of 1 mg/mL salmon sperm DNA (Sigma, Schnellendorf, Germany) and subsequently infected with Baculovirus-Luc at a multiplicity of infection (MOI) of 5. Cells were lysed 24 hrs post-infection using Cell Culture Lysis Reagent (Promega, Mannheim, Germany) and luciferase recorded using Luciferase Assay System and a GloMax[®]-Multi Detection System (Promega, Mannheim, Germany).

4.11. Murine Cytomegalovirus

NIH/3T3 cells were seeded at a density of 4×10^4 cells/well of a 48-well plate and allowed to attach overnight. On the next day, MCMV strain delm157-luc rep [41] was adsorbed to cells (MOI 0.5) at 4 °C in the presence of 1 and 10 µM TAT-I24 with the aid of centrifugal enhancement twice at $800 \times g$ for 15 min. After 1.5 h incubation at 4 °C, the medium was removed and cells washed three times with ice-cold medium before transfer to 37 °C. After the indicated time points, cells were lysed and DNA extracted using QIAmp DNA Mini kit (Qiagen, Hilden, Germany) for subsequent PCR analysis using the primers luciferase for 5'-TGGAGAGCAACTGCATAAGG-3' (250 nM), luciferase rev: 5'-CGTTTCATAGCTTCTGCCAA-3' (250 nM) and normalised to 18S DNA using Luna[®] Universal qPCR Mastermix (New England BioLabs, Frankfurt am Main, Germany) as described previously [23].

4.12. Bromodeoxyuridine-Labelled MCMV and Microscopy

NIH/3T3 cells were seeded at a density of 4×10^5 cells/well of a 6-well plate and infected with murine MCMV strain delm157-luc rep [41] at an MOI of 10. After 24 h, the medium was removed and replaced with a medium containing 10 µM bromodeoxyuridine (BrdU). After 72 h, BrdU was added to the medium again. After 96 h, supernatants were harvested, cleared by centrifugation and directly used for infection [54]. NIH/3T3 cells were seeded at a density of 4×10^4 cells/well of ibiTreat 8-well chambers (ibidi, Germany). BrdU-labelled MCMV (MOI 0.25) was adsorbed to cells at 4 °C in the absence or presence of 10 µM TAT-I24 with the aid of centrifugal enhancement ($800 \times g$; 2×15 min at 4 °C). After 1.5 h, cells were washed three times with an ice-cold medium before returning the slides to 37 °C. Cells were fixed either before temperature shift (0 min) or 15 and 60 min after post-cold release with 5% formaldehyde for 10 min followed by permeabilization with PBS + 0.5% Triton X-100 (Sigma, Schnellendorf, Germany) for 10 min. In another setting, cells were infected with BrdU-labelled MCMV for one hour followed by fixation and permeabilization of the cells. One well was then incubated with 10 µM TAT-I24 for one hour before washing and further processing of the slides.

BrdU-labelled MCMV was also adsorbed to NIH/3T3 cells in the presence of 5 µM FAM-TAT-I24 at 4 °C for 1.5 h with the aid of centrifugal enhancement. Cells were then washed three times with an ice-cold medium and incubated at 37 °C for 30 min. Cells were then fixed and permeabilised as described above.

Staining for BrdU was performed by incubation of cells with 1 N HCl for 30 min at 37 °C followed by removal of the HCl and incubation of the slides twice with $1 \times$ Tris-borate EDTA (TBE) buffer for neutralization. Staining was performed with a mouse monoclonal anti-BrdU antibody (#B8434; Sigma-Aldrich Schnellendorf, Germany) 1:250 diluted in PBS + 1% FCS overnight at 4 °C and a goat anti-mouse IgG-Texas Red (#T6390; ThermoFisher, Darmstadt, Germany) 1:100 diluted followed by staining of the nuclei with 4',6-Diamidin-2-phenylindol (DAPI). Microscopic examination was performed using a Live Cell Video Microscope (Leica Microsystems, Wetzlar, Germany).

COS-7 cells were seeded at a density of 2.5×10^4 cells/well into ibiTreat 8-well chambers and treated on the next day with TAT-I24 (20 μ M) in the absence or presence of 1 mg/mL salmon sperm DNA. After 1 h, cells were fixed with 5% formaldehyde. Microscopic examination was performed using a Live Cell Video Microscope (Leica Microsystems, Wetzlar, Germany).

4.13. Molecular Modelling

4.13.1. Setup of Structures and Geometries

The NMR structure of the TAT/RNA complex (pdb 6MCE, model-1; [35]) was taken as a template and RNA nucleotides substituted with DNA nucleotides. AMBER-18 [55] was used throughout working with force fields, protein.ff14SB, DNA.bsc1, water.tip3p and ion-sjc_tip3. An initial correspondence between 6MCE nucleotides and target positions in the ds (AT/GC) hairpin oligonucleotides was established as follows, 5'-C₁₉A₂₀T₂₁A₂₂T₂₆A₂₇T₂₈-A₂₉T₃₀C₃₁C₃₂C₃₃C₃₄A₃₅T₃₆A₃₇T₃₈A₃₉T₄₀A₄₁T₄₂G₄₃-3' and 5'-C₁₉G₂₀C₂₁G₂₂C₂₆G₂₇C₂₈G₂₉-C₃₀T₃₁T₃₂T₃₃T₃₄G₃₅C₃₆G₃₇C₃₈G₃₉C₄₀G₄₁C₄₂G₄₃-3' where subscripts denote residue numbers in the original 6MCE structure. It follows that 3 terminal nucleotides were discarded from the original 6MCE pdb file at both the 5' and 3' end to arrive at the anticipated oligonucleotides forming 22-mer hairpin structures. For adjustment of the target peptide sequence, the 4 N-terminal amino acid residues in 6MCE were discarded and the 2nd/3rd-last residues at the C-terminal end were converted from Ala-His to Pro-Pro. Optionally, the 9-mer peptide I24 (CLAFYACFC) was added in α -helical conformation (as revealed from long term MD simulation in aqueous solution) at the C-terminal end. Restrained vacuum minimization (20,000 steps) was carried out using 19/27 distance restraints between H-bond forming atoms of purine/pyrimidine base pairs. This was followed by a series of 5 short term restrained equilibration runs in a vacuum (250 ps) to relax ds (AT/GC) hairpin geometries. VMD [56] was used for graphical control whenever necessary.

4.13.2. Minimization, Equilibration, Production MD

Relaxed structures were neutralised with Na⁺ ions and embedded in explicit water (TIP3P [57]) using a minimum distance of 15 Å between any peptide/DNA atom and the border of the box. 500 steps of steepest descent minimization were performed with program SANDER followed by another 500 steps of conjugate gradient minimization including distance restraints and a cut-off of 12 Å. Minimised structures were heated to 300 K within 100 ps of equilibration MD using Langevin dynamics in the NTV ensemble and upheld distance restraints (program pmemd.MPI). Particle mesh Ewald summation was applied (cut off the radius of 12 Å, time step 1 fs) and bonds involving H-atoms were considered by the SHAKE algorithm [58]. Continuing with endpoint structures another 200 ps of equilibration MD were carried out at identical conditions except that pressure coupling was introduced (ntb = 2, ntp = 1, barostat = 2, taup = 2.0). This was followed by another 100 ps of equilibration MD during which distance restraints were dropped and additional 500 ps to switch from pmemd.MPI to program pmemd.cuda at otherwise identical conditions. Equilibrated systems were taken up for production MD at identical simulation conditions. Overall sampling time was 250 ns in production runs.

4.13.3. MM/PBSA

Following previous studies by Sim et al., 2017 [36] binding free energies were computed using the MM/PBSA approach [37]. Only single trajectories were taken into account, i.e., the simulation of the peptide/DNA-complex was serving for both the bound as well as the isolated receptor/ligand states. The [ante-]MMPBSA.py scripts provided in AMBER-18 were used. For continuum electrostatics both PB and GB models were applied with corresponding name list entries (igb = 5, saltcon = 0.047088/0.045673) and (inp = 1, radiopt = 0, istrng = 0.047088/0.045673) where ionic strengths mentioned above/below the bar are to be seen for ds (AT) and ds (GC) systems respectively. Entropic contributions were considered as well but evaluations were carried out independently with and without them. Owing

to the significant degree of structural re-arrangement occurring in the initial stage of MD simulation, multiple evaluations were carried out considering varying intervals from the simulation endpoint.

4.14. Data Analysis

Statistical analysis was performed using GraphPad Prism 8 (GraphPad Software, San Diego, CA, USA).

5. Patents

Hanna Harant is the inventor of patent application WO2019/057973 “Gene expression inhibitors”.

Supplementary Materials: The following are available online at <https://www.mdpi.com/article/10.3390/biologics1010003/s1>. Figure S1: Structural information of the TAT protein as a template for affinity studies. Figure S2: Structural sample, TAT-I24/ds (AT). Figure S3: Fluorescence emission of a complex of TAT-I24 with DNA. Table S1: Binding affinities of TAT or TAT-I24. Video S1: Conformational dynamics of TAT-I24 DNA complexes.

Author Contributions: Conceptualization, H.H. (Hanna Harant), S.H., F.K. and I.J.D.L.; methodology, H.H. (Hanna Harant), S.H., F.K., C.R. and Z.R.; software, S.H.; validation, H.H. (Hanna Harant), S.H., F.K., Z.R., H.H. (Hartmut Hengel) and I.J.D.L.; formal analysis, H.H. (Hanna Harant), I.J.D.L. and H.H. (Hartmut Hengel); investigation, H.H. (Hanna Harant), S.H. and F.K.; writing—original draft preparation, H.H. (Hanna Harant) and S.H.; writing—review and editing, S.H., F.K., H.H. (Hartmut Hengel) and I.J.D.L.; project administration, H.H. (Hanna Harant); funding acquisition, H.H. (Hanna Harant). All authors have read and agreed to the published version of the manuscript.

Funding: This research was funded by PreSeed (P1812709-PSL01) of BMDW resp., BMVIT, handled by aws (Austria Wirtschaftsservice).

Data Availability Statement: The data presented in this study are available on request from the corresponding author.

Acknowledgments: We wish to thank Irina Korschineck for her continuous support throughout the project. We also thank Simone Gruber for virus titration.

Conflicts of Interest: Hanna Harant holds 100% of the shares of Pivaris BioScience GmbH. The other authors declare no conflict of interest.

References

1. Adalja, A.; Inglesby, T. Broad-Spectrum Antiviral Agents: A Crucial Pandemic Tool. *Expert Rev. Anti Infect. Ther.* **2019**, *17*, 467–470. [[CrossRef](#)]
2. Chitalia, V.C.; Munawar, A.H. A painful lesson from the COVID-19 pandemic: The need for broad-spectrum, host-directed antivirals. *J. Transl. Med.* **2020**, *18*, 390. [[CrossRef](#)]
3. Zhu, J.-D.; Meng, W.; Wang, X.-J.; Wang, H.-C.R. Broad-spectrum antiviral agents. *Front. Microbiol.* **2015**, *6*, 1–15. [[CrossRef](#)]
4. Qureshi, A.; Tandon, H.; Thakur, N.; Kumar, M. AVpdb: A database of experimentally validated antiviral peptides targeting medically important viruses. *Nucleic Acids Res.* **2013**, *42*, D1147–D1153. [[CrossRef](#)]
5. Vilas Boas, L.C.P.; Campos, M.L.; Berlanda, R.L.A.; de Carvalho Neves, N.; Franco, O.L. Antiviral peptides as promising therapeutic drugs. *Cell. Mol. Life Sci.* **2019**, *76*, 3525–3542. [[CrossRef](#)]
6. Ahmed, A.; Siman-Tov, G.; Hall, G.; Bhalla, N.; Narayanan, A. Human Antimicrobial Peptides as Therapeutics for Viral Infections. *Viruses* **2019**, *11*, 704. [[CrossRef](#)]
7. Agarwal, G.; Gabrani, R. Antiviral Peptides: Identification and Validation. *Int. J. Pept. Res. Ther.* **2021**, *27*, 149–168. [[CrossRef](#)] [[PubMed](#)]
8. Skalickova, S.; Heger, Z.; Krejcova, L.; Pekarik, V.; Bastl, K.; Janda, J.; Kostolansky, F.; Vareckova, E.; Zitka, O.; Adam, V.; et al. Perspective of Use of Antiviral Peptides against Influenza Virus. *Viruses* **2015**, *7*, 5428–5442. [[CrossRef](#)] [[PubMed](#)]
9. Zhao, H.; To, K.K.W.; Sze, K.-H.; Yung, T.T.-M.; Bian, M.; Lam, H.; Yeung, M.L.; Li, C.; Chu, H.; Yuen, K.-Y. A broad-spectrum virus- and host-targeting peptide against respiratory viruses including influenza virus and SARS-CoV-2. *Nat. Commun.* **2020**, *11*, 4252. [[CrossRef](#)] [[PubMed](#)]
10. Jones, J.C.; Turpin, E.A.; Bultmann, H.; Schultz-Cherry, S.; Brandt, C.R. Inhibition of Influenza Virus Infection by a Novel Antiviral Peptide That Targets Viral Attachment to Cells. *J. Virol.* **2006**, *80*, 11960–11967. [[CrossRef](#)]

11. Altmann, S.E.; Jones, J.C.; Schultz-Cherry, S.; Brandt, C.R. Inhibition of Vaccinia virus entry by a broad spectrum antiviral peptide. *Virology* **2009**, *388*, 248–259. [[CrossRef](#)]
12. Nicol, M.Q.; Ligertwood, Y.; Bacon, M.N.; Dutia, B.M.; Nash, A.A. A novel family of peptides with potent activity against influenza A viruses. *J. Gen. Virol.* **2012**, *93*, 980–986. [[CrossRef](#)]
13. Kadam, R.U.; Juraszek, J.; Brandenburg, B.; Buyck, C.; Schepens, W.B.G.; Kesteleyn, B.; Stoops, B.; Vreeken, R.J.; Vermond, J.; Goutier, W.; et al. Potent peptidic fusion inhibitors of influenza virus. *Science* **2017**, *358*, 496–502. [[CrossRef](#)] [[PubMed](#)]
14. Xia, S.; Yan, L.; Xu, W.; Agrawal, A.S.; Algaissi, A.; Tseng, C.-T.K.; Wang, Q.; Du, L.; Tan, W.; Wilson, I.A.; et al. A pan-coronavirus fusion inhibitor targeting the HR1 domain of human coronavirus spike. *Sci. Adv.* **2019**, *5*, eaav4580. [[CrossRef](#)] [[PubMed](#)]
15. Xia, S.; Liu, M.; Wang, C.; Xu, W.; Lan, Q.; Feng, S.; Qi, F.; Bao, L.; Du, L.; Liu, S.; et al. Inhibition of SARS-CoV-2 (previously 2019-nCoV) infection by a highly potent pan-coronavirus fusion inhibitor targeting its spike protein that harbors a high capacity to mediate membrane fusion. *Cell Res.* **2020**, *30*, 343–355. [[CrossRef](#)] [[PubMed](#)]
16. Wimley, W.C.; White, S.H. Experimentally determined hydrophobicity scale for proteins at membrane interfaces. *Nat. Struct. Mol. Biol.* **1996**, *3*, 842–848. [[CrossRef](#)]
17. Badani, H.; Garry, R.F.; Wimley, W.C. Peptide entry inhibitors of enveloped viruses: The importance of interfacial hydrophobicity. *Biochim. Biophys. Acta - Biomembr.* **2014**, *1838*, 2180–2197. [[CrossRef](#)]
18. Hoffmann, A.R.; Guha, S.; Wu, E.; Ghimire, J.; Wang, Y.; He, J.; Garry, R.F.; Wimley, W.C. Broad-Spectrum Antiviral Entry Inhibition by Interfacially Active Peptides. *J. Virol.* **2020**, *94*, 1–20. [[CrossRef](#)]
19. Thakur, N.; Qureshi, A.; Kumar, M. AVPpred: Collection and prediction of highly effective antiviral peptides. *Nucleic Acids Res.* **2012**, *40*, 199–204. [[CrossRef](#)]
20. Chowdhury, A.S.; Reehl, S.M.; Kehn-Hall, K.; Bishop, B.; Webb-Robertson, B.J.M. Better understanding and prediction of antiviral peptides through primary and secondary structure feature importance. *Sci. Rep.* **2020**, *10*, 1–8. [[CrossRef](#)]
21. Matthews, T.; Salgo, M.; Greenberg, M.; Chung, J.; DeMasi, R.; Bolognesi, D. Enfuvirtide: The first therapy to inhibit the entry of HIV-1 into host CD4 lymphocytes. *Nat. Rev. Drug Discov.* **2004**, *3*, 215–225. [[CrossRef](#)]
22. Blank, A.; Markert, C.; Hohmann, N.; Carls, A.; Mikus, G.; Lehr, T.; Alexandrov, A.; Haag, M.; Schwab, M.; Urban, S.; et al. First-in-human application of the novel hepatitis B and hepatitis D virus entry inhibitor myrcludex B. *J. Hepatol.* **2016**, *65*, 483–489. [[CrossRef](#)] [[PubMed](#)]
23. Ruzsics, Z.; Hoffmann, K.; Riedl, A.; Krawczyk, A.; Widera, M.; Sertznig, H.; Schipper, L.; Kapper-Falcone, V.; Debreczeny, M.; Ernst, W.; et al. A Novel, Broad-Acting Peptide Inhibitor of Double-Stranded DNA Virus Gene Expression and Replication. *Front. Microbiol.* **2020**, *11*, 2934. [[CrossRef](#)] [[PubMed](#)]
24. Shi, Y.B.; Gamper, H.; Hearst, J.E. Interaction of T7 RNA polymerase with DNA in an elongation complex arrested at a specific psoralen adduct site. *J. Biol. Chem.* **1988**, *263*, 527–534. [[CrossRef](#)]
25. Place, C.; Oddos, J.; Buc, H.; McAllister, W.T.; Buckle, M. Studies of contacts between T7 RNA polymerase and its promoter reveal features in common with multisubunit RNA polymerases. *Biochemistry* **1999**, *38*, 4948–4957. [[CrossRef](#)] [[PubMed](#)]
26. Yindeeyoungyeon, W.; Schell, M.A. Footprinting with an Automated Capillary DNA Sequencer. *Biotechniques* **2000**, *29*, 1034–1041. [[CrossRef](#)]
27. Severinov, K.; Darst, S.A. A mutant RNA polymerase that forms unusual open promoter complexes. *Proc. Natl. Acad. Sci. USA* **1997**, *94*, 13481–13486. [[CrossRef](#)] [[PubMed](#)]
28. Green, M.; Loewenstein, P.M. Autonomous functional domains of chemically synthesized human immunodeficiency virus tat trans-activator protein. *Cell* **1988**, *55*, 1179–1188. [[CrossRef](#)]
29. Vivès, E.; Brodin, P.; Lebleu, B. A Truncated HIV-1 Tat Protein Basic Domain Rapidly Translocates through the Plasma Membrane and Accumulates in the Cell Nucleus. *J. Biol. Chem.* **1997**, *272*, 16010–16017. [[CrossRef](#)]
30. Ignatovich, I.A.; Dizhe, E.B.; Pavlotskaya, A.V.; Akifiev, B.N.; Burov, S.V.; Orlov, S.V.; Perevozchikov, A.P. Complexes of Plasmid DNA with Basic Domain 47–57 of the HIV-1 Tat Protein Are Transferred to Mammalian Cells by Endocytosis-mediated Pathways. *J. Biol. Chem.* **2003**, *278*, 42625–42636. [[CrossRef](#)]
31. Ziegler, A.; Seelig, J. High affinity of the cell-penetrating peptide HIV-1 Tat-PTD for DNA. *Biochemistry* **2007**, *46*, 8138–8145. [[CrossRef](#)]
32. Lv, M.X.; Duan, B.C.; Lu, K.; Wu, Y.J.; Zhao, Y.F. Synthesis, DNA-Binding and Antibacterial Activity of the Cell-Penetrating Peptide HIV-1 Tat (49–57). *Indian J. Pharm. Sci.* **2017**, *79*, 893–899. [[CrossRef](#)]
33. Hsu, C.-H. Structural and DNA-binding studies on the bovine antimicrobial peptide, indolicidin: Evidence for multiple conformations involved in binding to membranes and DNA. *Nucleic Acids Res.* **2005**, *33*, 4053–4064. [[CrossRef](#)] [[PubMed](#)]
34. Schulze-Gahmen, U.; Hurley, J.H. Structural mechanism for HIV-1 TAR loop recognition by Tat and the super elongation complex. *Proc. Natl. Acad. Sci. USA* **2018**, *115*, 12973–12978. [[CrossRef](#)]
35. Pham, V.V.; Salguero, C.; Khan, S.N.; Meagher, J.L.; Brown, W.C.; Humbert, N.; de Rocquigny, H.; Smith, J.L.; D'Souza, V.M. HIV-1 Tat interactions with cellular 7SK and viral TAR RNAs identifies dual structural mimicry. *Nat. Commun.* **2018**, *9*, 4266. [[CrossRef](#)]
36. Sim, S.; Wang, P.; Beyer, B.N.; Cutrona, K.J.; Radhakrishnan, M.L.; Elmore, D.E. Investigating the nucleic acid interactions of histone-derived antimicrobial peptides. *FEBS Lett.* **2017**, *591*, 706–717. [[CrossRef](#)] [[PubMed](#)]
37. Kollman, P.A.; Massova, I.; Reyes, C.; Kuhn, B.; Huo, S.; Chong, L.; Lee, M.; Lee, T.; Duan, Y.; Wang, W.; et al. Calculating Structures and Free Energies of Complex Molecules: Combining Molecular Mechanics and Continuum Models. *Acc. Chem. Res.* **2000**, *33*, 889–897. [[CrossRef](#)] [[PubMed](#)]

38. Kar, P.; Seel, M.; Weidemann, T.; Höfinger, S. Theoretical mimicry of biomembranes. *FEBS Lett.* **2009**, *583*, 1909–1915. [[CrossRef](#)] [[PubMed](#)]
39. Kar, P.; Seel, M.; Hansmann, U.H.E.; Höfinger, S. Dispersion Terms and Analysis of Size- and Charge Dependence in an Enhanced Poisson–Boltzmann Approach. *J. Phys. Chem. B* **2007**, *111*, 8910–8918. [[CrossRef](#)] [[PubMed](#)]
40. Mahajan, R.; Kranzlmüller, D.; Volkert, J.; Hansmann, U.H.E.; Höfinger, S. Computational assessment of the entropy of solvation of small-sized hydrophobic entities. *Phys. Chem. Chem. Phys.* **2006**, *8*, 5515–5521. [[CrossRef](#)]
41. Trilling, M.; Le, V.T.K.; Fiedler, M.; Zimmermann, A.; Bleifuß, E.; Hengel, H. Identification of DNA-Damage DNA-Binding Protein 1 as a Conditional Essential Factor for Cytomegalovirus Replication in Interferon- γ -Stimulated Cells. *PLoS Pathog.* **2011**, *7*, e1002069. [[CrossRef](#)]
42. Loughran, S.P.; McCrudden, C.M.; McCarthy, H.O. Designer peptide delivery systems for gene therapy. *Eur. J. Nanomed.* **2015**, *7*, 85–96. [[CrossRef](#)]
43. Bultmann, H.; Brandt, C.R. Peptides Containing Membrane-transiting Motifs Inhibit Virus Entry. *J. Biol. Chem.* **2002**, *277*, 36018–36023. [[CrossRef](#)]
44. Bultmann, H.; Teuton, J.; Brandt, C.R. Addition of a C-terminal cysteine improves the anti-herpes simplex virus activity of a peptide containing the human immunodeficiency virus type 1 TAT protein transduction domain. *Antimicrob. Agents Chemother.* **2007**, *51*, 1596–1607. [[CrossRef](#)]
45. Lundberg, M.; Wikström, S.; Johansson, M. Cell surface adherence and endocytosis of protein transduction domains. *Mol. Ther.* **2003**, *8*, 143–150. [[CrossRef](#)]
46. Richard, J.P.; Melikov, K.; Brooks, H.; Prevot, P.; Lebleu, B.; Chernomordik, L.V. Cellular uptake of unconjugated TAT peptide involves clathrin-dependent endocytosis and heparan sulfate receptors. *J. Biol. Chem.* **2005**, *280*, 15300–15306. [[CrossRef](#)]
47. Lo, S.L.; Wang, S. An endosomolytic Tat peptide produced by incorporation of histidine and cysteine residues as a nonviral vector for DNA transfection. *Biomaterials* **2008**, *29*, 2408–2414. [[CrossRef](#)]
48. Jeong, C.; Yoo, J.; Lee, D.; Kim, Y.-C. A branched TAT cell-penetrating peptide as a novel delivery carrier for the efficient gene transfection. *Biomater. Res.* **2016**, *20*, 28. [[CrossRef](#)]
49. Wilson, S.S.; Wiens, M.E.; Smith, J.G. Antiviral Mechanisms of Human Defensins. *J. Mol. Biol.* **2013**, *425*, 4965–4980. [[CrossRef](#)]
50. Hazrati, E.; Galen, B.; Lu, W.; Wang, W.; Ouyang, Y.; Keller, M.J.; Lehrer, R.I.; Herold, B.C. Human α - and β -Defensins Block Multiple Steps in Herpes Simplex Virus Infection. *J. Immunol.* **2006**, *177*, 8658–8666. [[CrossRef](#)]
51. Zhao, H.; Zhou, J.; Zhang, K.; Chu, H.; Liu, D.; Poon, V.K.-M.; Chan, C.C.-S.; Leung, H.-C.; Fai, N.; Lin, Y.-P.; et al. A novel peptide with potent and broad-spectrum antiviral activities against multiple respiratory viruses. *Sci. Rep.* **2016**, *6*, 22008. [[CrossRef](#)]
52. Pul, Ü.; Wurm, R.; Wagner, R. KMnO₄ Footprinting. *Bio-Protocol* **2012**, *2*, 1–5. [[CrossRef](#)]
53. Hausner, W.; Thomm, M. Events during initiation of archaeal transcription: Open complex formation and DNA-protein interactions. *J. Bacteriol.* **2001**, *183*, 3025–3031. [[CrossRef](#)]
54. Rosenke, K.; Fortunato, E.A. Bromodeoxyuridine-Labeled Viral Particles as a Tool for Visualization of the Immediate-Early Events of Human Cytomegalovirus Infection. *J. Virol.* **2004**, *78*, 7818–7822. [[CrossRef](#)]
55. Case, D.A.; Ben-Shalom, I.Y.; Brozell, S.R.; Cerutti, D.S.; Cheatham, T.E.I.; Cruzeiro, V.W.D.; Darden, T.; Duke, R.E.; Ghoreishi, D.; Gilson, M.K.; et al. *Amber 18*; University of California: San Francisco, CA, USA, 2018.
56. Humphrey, W.; Dalke, A.; Schulten, K. VMD: Visual molecular dynamics. *J. Mol. Graph.* **1996**, *14*, 33–38. [[CrossRef](#)]
57. Jorgensen, W.L.; Chandrasekhar, J.; Madura, J.D.; Impey, R.W.; Klein, M.L. Comparison of simple potential functions for simulating liquid water. *J. Chem. Phys.* **1983**, *79*, 926–935. [[CrossRef](#)]
58. van Gunsteren, W.F.; Berendsen, H.J.C. Algorithms for macromolecular dynamics and constraint dynamics. *Mol. Phys.* **1977**, *34*, 1311–1327. [[CrossRef](#)]